



OPEN

Dislocation creation and void nucleation in FCC ductile metals under tensile loading: A general microscopic picture

SUBJECT AREAS:
STRUCTURE OF SOLIDS
AND LIQUIDS
ATOMISTIC MODELSWei-Wei Pang^{1,2}, Ping Zhang^{1,2}, Guang-Cai Zhang¹, Ai-Guo Xu¹ & Xian-Geng Zhao¹Received
1 September 2014Accepted
21 October 2014Published
10 November 2014Correspondence and
requests for materials
should be addressed to
P.Z. (zhang_ping@
iapcm.ac.cn) or
G.-C.Z.
(zhang_guangcai@
iapcm.ac.cn)¹Institute of Applied Physics and Computational Mathematics, Beijing 100088, People's Republic of China, ²Beijing Computational Science Research Center, Beijing 100089, People's Republic of China.

Numerous theoretical and experimental efforts have been paid to describe and understand the dislocation and void nucleation processes that are fundamental for dynamic fracture modeling of strained metals. To date an essential physical picture on the self-organized atomic collective motions during dislocation creation, as well as the essential mechanisms for the void nucleation obscured by the extreme diversity in structural configurations around the void nucleation core, is still severely lacking in literature. Here, we depict the origin of dislocation creation and void nucleation during uniaxial high strain rate tensile processes in face-centered-cubic (FCC) ductile metals. We find that the dislocations are created through three distinguished stages: (i) Flattened octahedral structures (FOSs) are randomly activated by thermal fluctuations; (ii) The double-layer defect clusters are formed by self-organized stacking of FOSs on the close-packed plane; (iii) The stacking faults are formed and the Shockley partial dislocations are created from the double-layer defect clusters. Whereas, the void nucleation is shown to follow a two-stage description. We demonstrate that our findings on the origin of dislocation creation and void nucleation are universal for a variety of FCC ductile metals with low stacking fault energies.

The stretch loading and shock unloading damage processes of ductile metals involve complicated generation and evolution of a series of microscopic structures such as dislocations and voids^{1–3}, a deep knowledge on which composes the most fundamental basis for a predictive dynamic fracture modeling. At low and mediate strain rates, it is generally believed that due to the fact that the material is mechanically near equilibrium and experiences a process of low energy state, these microscopic structures are created in the energetically activated regions (grain boundary, for instance) manifested by atomic deviations from ideal crystal lattice sites. At high strain rates, however, because the inertia becomes to play a crucial role, there is no time enough to release the local stresses. In this case, striking mechanical non-equilibrium drives the material to experience various excited high energy states. As a response, the dislocations and voids can be generated in the interior of bulk crystal with the help of thermal fluctuations as well as phonon softening.

To describe and understand the dislocation creation and void nucleation processes that the present experimental advances are still extremely difficult to catch the microscopic mechanism, numerous theoretical efforts, mainly through molecular dynamics simulations, have been paid in the last decade. Void surface⁴, crack tip⁵, energetic atomic clusters with larger relative displacements⁶, bicrystal interfaces⁷, grain boundaries⁸, as well as free surfaces^{9,10}, have been shown to provide reliable activated volumes for dislocation nucleation driven by critical local shear stress. Most of these studies were mainly focused on the conditions and influential factors responsible for dislocation nucleation with the aim to provide explanative clues to understand critical yield phenomena and the corresponding microscopic plasticity. Whereas, to date an essential physical picture on the self-organized atomic collective motions during dislocation nucleation keeps unclear. The reason is that no effective description of universal sense has been given to classify the complicated atomic configurations of dislocations within the activated volume. For void nucleation, it has been acknowledged that under low strain rate or quasi static stretching, voids occur predominantly via the second-phase particle cracking or second-phase debonding from the matrix material¹¹. Under the moderate stretching, voids nucleate preferentially at the grain boundary junctions and grow along the grain boundary^{12,13}. At high strain rates, various microscopic or mesoscopic voids may evolve both on the grain boundaries^{14,15} and inside the bulk crystal¹⁶. These results prove to be indispensable for understanding the onset and development of dynamic damage. Again, however, due to the very scarce knowledge on the extreme diversity in structural configurations around the void nucleation core, a general description on the



shapes and distribution of nucleated voids, thus the reliable mechanisms for void nucleation, are still severely lacking.

Inspired by the above-mentioned observation, in the present paper, as a first step we try to understand the atomic self-organized collective motion law for the dislocation creation and clarify the mechanisms for the void nucleation at high strain rate. For this aim, in our molecular dynamics simulations we choose to select single-crystal FCC metals, in which because the atoms are in order, the newly created microscopic structures are possible to be identified and tracked, and because the stress is uniform, the creation mechanisms for the microscopic structures are feasible to be analyzed. We give a three-stage picture on the dislocation creation: (i) The FOSs (see below for definition) are firstly activated by thermal fluctuations; (ii) The double-layer defect clusters are formed by self-organized stacking of FOSs on the close-packed plane; (iii) The stacking faults are formed by the slip of atoms within the defect clusters and the Shockley partial dislocations are created. These three stages for dislocation creation have their distinguished structure characters, and they are clearly separated in the time domain. We also propose a two-stage mechanism for the void nucleation: (i) The vacancy strings are firstly formed by intersection of two stacking faults; (ii) Then the vacancy strings transform into the voids by emitting dislocations. We show that these general findings can be applied to a variety of FCC ductile metals with low stacking fault energies.

Results

The materials we use for simulations include Ag, Au, Cu, Ni, Pt, and Pd. These metals have a low stacking fault energy. The simulation tool is the well-known LAMMPS software package¹⁷. The interatomic interaction is described by an embedded atom method (EAM) potential^{18,19}. The simulation box consists of $80 \times 80 \times 80$ unit cells and contains approximately 2×10^6 atoms. Periodic boundary conditions are used to minimize surface and edge effects. The system is initially equilibrated at ambient pressure $P = 0$ GPa. If not explicitly mentioned, the initial temperature is set at 3 K. Once the equilibrium is established, the thermostat is turned off and the uniaxial tensile strain is applied along the [100] direction with two constant strain rates $\dot{\epsilon} = 10^9/s$ and $10^8/s$ for comparison. The atoms are distinguished by calculating their coordination numbers and common neighbor analysis (CNA) values.

During the early stage of loading, the system responds elastically and the lattices are stretched without dislocations formed. As the strain increases, some atoms deviate from their equilibrium lattice positions to form defect clusters, as shown in Fig. 1(a). Strikingly, most of these atomic clusters form what we henceforth call flattened octahedral structures (FOSs). The six vertex atoms of a FOS are the face-centered atoms of the FCC crystal, see the top right inset in Fig. 1(a). The formation of FOSs can be understood as follows: Under the tensile loading along the x direction, to remain the minimum energy state, two face-centered atoms along the z or the y axis become closer. The shifts of these two atoms lead to that they become neighboring atoms and simultaneously change the CNA values of other four atoms. Therefore, the FOS can be identified by the CNA value. When the strain is small, the FOSs are sparse and randomly distributed. The FOSs are dynamical in that they may stochastically occur, annihilate, and reoccur in other places, reflecting their thermal fluctuation feature. Here, we point out that Poisson effect under the present uniaxial strain loading is reflected by the weakening of lattice stability, instead of lattice shrinking perpendicular to the loading direction. This weakening is characterized by phonon softening. The phonon modes with the wave vectors around $\mathbf{k} = (0, \pi/a, 0)$ or $\mathbf{k} = (0, 0, \pi/a)$ are softened, corresponding to the atomic movement in forming FOS. The potential barrier for the formation of the FOS structure decreases. Thus, the phonon softening allies thermal fluctuation to initiate the formation of FOS.

With increasing the stress, in the zones with cumulative FOSs, some FOSs tend to stack on the close-packed plane to form double-layer defect clusters, see Fig. 1(b) and the top left inset inside. This stacking process can be understood as follows: The FOSs attract with each other in tensile FCC metal, leading to the atoms other than the collapsed atoms of the FOSs to also collapse to form more FOSs that stack on the same close-packed plane, see the top right inset in Fig. 1(b). We calculate the Burgers vector of the double-layer defect clusters according to the Frank scheme²⁰, see the bottom left inset in Fig. 1(b), in which the blue loop is used to calculate the Burgers vector. The Burgers vector is determined to be $\mathbf{b} = [000]$, which demonstrates that the stacked FOSs initially form defect clusters other than stacking faults, and therefore no dislocations form at this FOS stacking stage.

When the size of the double-layer defect cluster exceeds a certain value, the central-region atoms of the cluster undergo a relative inter-layer slip. Such a process can be observed from two successive snapshots, Fig. 1(c) and Fig. 1(d), which are plotted in the way that one sees from the normal direction of close-packed plane. Before inter-layer slip [Fig. 1(c)], one can see that the two layers are mostly overlapped, leaving large slits (see the white region surround by black triangle for one slit). In Fig. 1(d), whereas, in the central region each slit is split into two little holes, while in the surrounding region, the slits remain the shape. This fact indicates that the central atoms in the double-layer defect cluster are more active than the atoms in the surroundings. We calculate the Burgers vector of the slipped double-layer defect cluster shown in Fig. 1(d), and find $\mathbf{b} = [1\bar{2}1]$ [see the top right inset in Fig. 1(e)]. The non-zero Burgers vector demonstrates that the dislocations are generated from the double-layer defect cluster due to the relative slip of the internal atoms.

After systematic calculations on the Burgers vectors of the nucleated dislocations in the simulation block, we find that these dislocations are all Shockley partial dislocations, such as $(111)\frac{1}{6}[1\bar{2}1]$ and $(\bar{1}\bar{1}\bar{1})\frac{1}{6}[\bar{1}12]$ shown in the inset in Fig. 1(e). It is well known that generally there are at most twelve types of Shockley partial dislocations to possibly appear in tensile FCC metals. In our simulations, however, we find that four types of partial dislocations, namely, $(111)\frac{1}{6}[\bar{2}11]$, $(\bar{1}\bar{1}\bar{1})\frac{1}{6}[\bar{2}\bar{1}\bar{1}]$, $(11\bar{1})\frac{1}{6}[\bar{2}1\bar{1}]$, and $(\bar{1}\bar{1}\bar{1})\frac{1}{6}[211]$, fail to occur. The reason is ultimately due to that under the present tensile loading along the [100] direction, no atoms along the [100] direction are collapsed to form the FOSs. Once small dislocations occur, they would grow up quickly and multiply to cover the whole simulation block, as shown in Fig. 1(f).

We stress that the above depiction on the origin of dislocation creation, particularly on the formation of FOSs and double-layer defect clusters, is insensitive to the loading direction. This can be seen from Fig. 2(a), which clearly show that the dislocation creation process under loading along the $[\bar{1}10]$ direction follows a similar three-stage description as that given in Fig. 1 for [100]-direction loading. Also, different setups for initial temperature and tensile strain rate do not change the above physical mechanism. Of course, with higher temperature set or higher strain rate set, more FOSs will be activated before dislocation creation, which can be seen from Fig. 2(b) and 2(c).

The dislocation nucleation and slip release part of the shear stress, but do not release bulk stress (negative pressure). As a result, with increasing the tensile strain, plenty of energies accumulate in the system. To release energy, some voids or cracks may be generated at the weak points in material. This is what we observe that the strain ultimately drives some voids to nucleate in dislocation aggregation regions, which are generally considered as weak points. Figure 3(a) shows the nucleated voids inside the simulation box. When loading along the [100] direction, the nucleation of voids is random inside

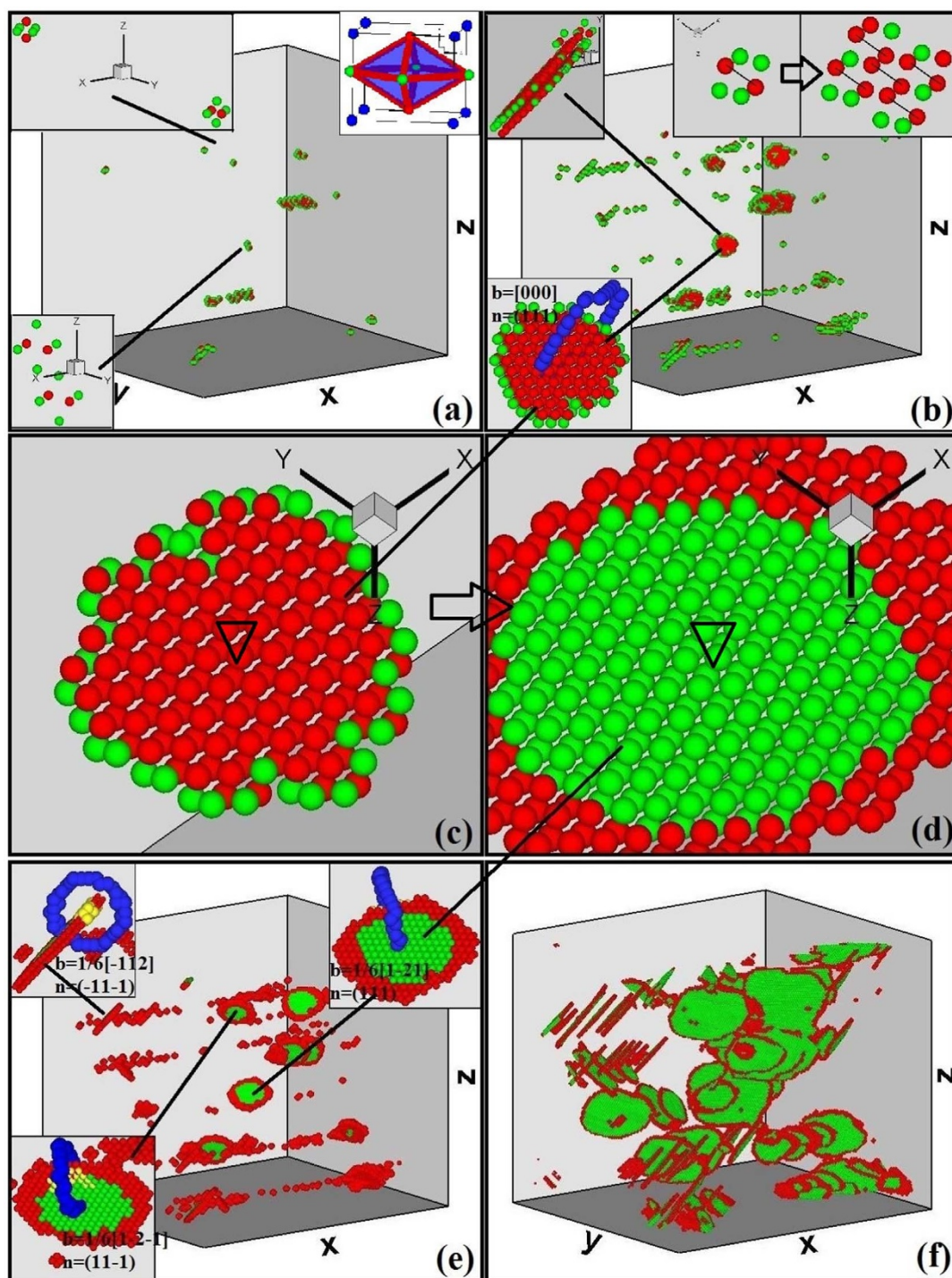


Figure 1 | Molecular-dynamics simulation snapshots that provide a general three-stage physical picture for the generation of dislocations and the corresponding non-zero Burgers vectors in FCC ductile metals under high-strain-rate uniaxial stretch. Panel (a) shows that FOSs (for a detailed view, see the top right inset) are firstly activated in the metals by thermal fluctuations. Panel (b) shows that FOSs begin to stack on the close-packed plane to form double-layer defect clusters (see the top left inset for closer view). This stacking process is shown in the top right inset. The Burgers vector for the double-layer defect cluster structure is calculated to be zero, as shown in the bottom left inset. Panel (c) and panel (d) shows the transformation of the double-layer defect clusters into stacking faults. Panel (e) gives a few non-zero Burgers vectors of the nucleated dislocations that surround the stacking faults. Panel (f) shows the growth of stacking faults and dislocations. In panels (a)–(c) the coordination numbers of red and green atoms are 13 and 12, respectively, while in panels (d)–(f) the CNA values of red and green atoms are 5 (dislocation atoms) and 2 (hcp atoms), respectively.

the simulation box and most incipient void shapes are found to be pillar-like. Figure 3(b) shows the nucleated voids from different views. Peculiarly, we find that the elongations of voids are predominantly along the $[011]$ and $[0\bar{1}1]$ directions that are perpendicular to the loading direction, while the voids of other directions do not grow up.

To further reveal the incipient nucleation mechanism of voids, we picked out a layer, with a thickness of 2.3 nm, perpendicular to the elongation direction of void. Figures 3(c)–(f) show the evolutionary process of these atoms in the layer, where only the defect atoms are shown and the direction of principal plane is $[0\bar{1}1]$, and therein the

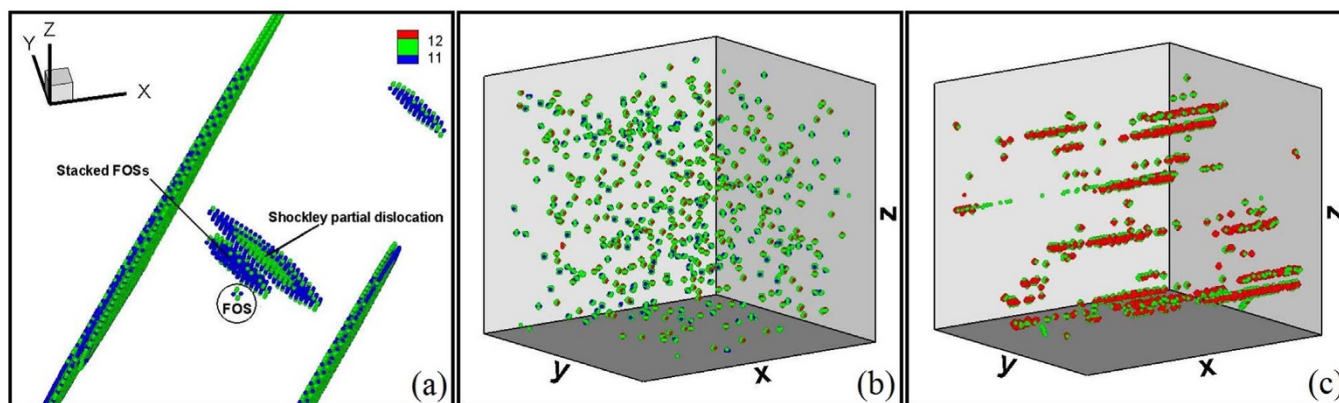


Figure 2 | Molecular-dynamics simulation snapshots for different setups from those in Fig. 1. Panel (a) shows the simulation results under loading along the $[110]$ direction. Panels (b) and (c) shows that compared to Fig. 1, more FOSs are activated with a higher initial temperature of 300 K or higher tensile strain rate of $\dot{\epsilon} = 10^9/s$.

insets are the schematic diagrams of stacking faults creation and vacancy string formation. When the tensile strain exceeds a certain value, crystal plastic deformation brings some stacking faults into the system, see Fig. 3(c) and the inset inside. Figure 3(c) shows four stacking faults which appear as lines in the present view. According to the Frank scheme, the left two stacking faults have the normal direction $[111]$ and the Burgers vector $\frac{1}{6}[12\bar{1}]$, while the right two ones have the normal direction $[1\bar{1}\bar{1}]$ and the Burgers vector $\frac{1}{6}[12\bar{1}]$. These stacking faults grow with time under the tensile loading. Meanwhile, stacking faults with different normal directions evolve to intersect with each other and generate pillar-like vacancy strings located at the intercrossing lines, see Fig. 3(d) and the inset inside. Figure 3(d) shows two vacancy strings (indicated by two black circles) resulting from the intersections of the left two and the right one stacking faults. These vacancy strings can grow into voids, provided dislocations are emitted from them. However, to emit dislocations, the size of vacancy string and the stress around the vacancy string must exceed some critical values. In Fig. 3(e) we could observe that the upper vacancy string grows up into a void via emitting dislocations, while the lower one retains its size. This is because there are more activated atoms around the upper vacancy string. The release of stress resulting from the growth of the nucleated voids will suppress the growth of neighboring vacancy strings. As a result, one can see from Fig. 3(f) that the nucleated void further grow and the other vacancy strings tend to disappear. In addition, We can also observe that the void shape gradually evolves from pillar-like into ellipsoidal.

The above process of vacancy string creation via the intersection of two stacking faults could be regarded as two successive plastic deformations. The first deformation brings a stacking fault into the system (see the inset in Fig. 3(c)), and the atoms have a displacement of the corresponding Burgers vector along the plane. During the second deformation process, the atoms further have a corresponding displacement along the other plane, which results in a volume variation (see the inset in Fig. 3(d)). The plastic deformation resulting from stacking faults can be described by a distortion tensor $\beta = \delta(\Sigma)\mathbf{b} = \iint_{\Sigma} ds' \delta(\mathbf{r}' - \mathbf{r})\mathbf{b}$, where $\delta(\Sigma)$ is the surface Dirac function, Σ is stacking fault plane, and \mathbf{b} is the Burgers vector. The relative volume variation is $\delta V/V = \text{Tr}(\beta)$. For the case of single stacking fault, $\text{Tr}(\beta) = \delta(\Sigma) \cdot \mathbf{b} = 0$, therefore, there is no density variation in the system. For the case of two stacking faults intersecting with each other, the distortion tensor is $\beta = \beta_1 + \beta_2 (\mathbf{I} + \beta_1)$, where β_1 and β_2 are the distortion tensors of the two stacking faults, respectively. Therefore, the volume variation is

$$\delta V = \int dV \text{Tr}(\beta_1 \cdot \beta_2) + (\mathbf{b}_2 \cdot \mathbf{n}_1)(\mathbf{b}_1 \cdot \mathbf{n}_2)L/|\mathbf{n}_1 \times \mathbf{n}_2|,$$

where \mathbf{n}_1 and \mathbf{n}_2 are normal directions of the stacking faults and L is the length of the vacancy string. Here, we arrive at that the cross-section area of vacancy string resulting from the intersection of two different stacking faults is $(\mathbf{b}_2 \cdot \mathbf{n}_1)(\mathbf{b}_1 \cdot \mathbf{n}_2)/|\mathbf{n}_1 \times \mathbf{n}_2|$, and the direction of vacancy string is $\mathbf{n}_1 \times \mathbf{n}_2$.

Since we have made it clear that the dislocations generated from the double-layer defect clusters are all Shockley partial dislocations, and the corresponding Burgers vectors have been obtained, then according to the above expression, we can determine that the initial vacancy strings have a typical cross-section area of $\sqrt{2}a^2/36$ (a is the lattice constant), and particularly, their distribution directions have six possible types. However, in Fig. 3(a) for voids evolved from vacancy strings, we only observe two types of voids with respective directions of $[011]$ and $[0\bar{1}1]$, which are perpendicular to the loading direction. This phenomenon can be qualitatively explained as follows: The energy released via growth of a vacancy string can be expressed as $\iint ds \cdot \sigma \cdot \delta \mathbf{r}$, where σ is the applied stress, s is the surface area of the vacancy string, and $\delta \mathbf{r}$ is the growth displacement. Since in our simulation setup the applied stress is σ_{xx} . Thus, only when the vacancy string is perpendicular to $[100]$, which enables it to have larger projective area along $[100]$, does its growth release more energy and evolve into voids. This analysis well explains the numerical results shown in Fig. 3(a).

We turn now to demonstrate that our present findings on the dislocation creation and void nucleation at high strain rates are universal for a variety of tensile FCC metals. For this purpose, we have simulated six types of FCC metals as mentioned above. The typical results are shown in Fig. 4, from which one can clearly see that although the number densities of nucleated voids are different in different metals, the nucleation processes show similar behaviors. Specially, we have verified that the initial FOS generation and stacking, dislocation creation and the corresponding Burgers vectors, vacancy string formation, as well as void shape and direction, are all analogous for the six metals. For example, as revealed in Fig. 4, under loading along $[100]$ direction most voids in all the six metals show pillar-like shapes, and their elongations are predominantly along the directions $[011]$ and $[0\bar{1}1]$.

Discussion

As a final remark, it should be noticed that all the metals under investigation in this work have low stacking fault energies. In these metals, the partial dislocations and stacking faults are initiated

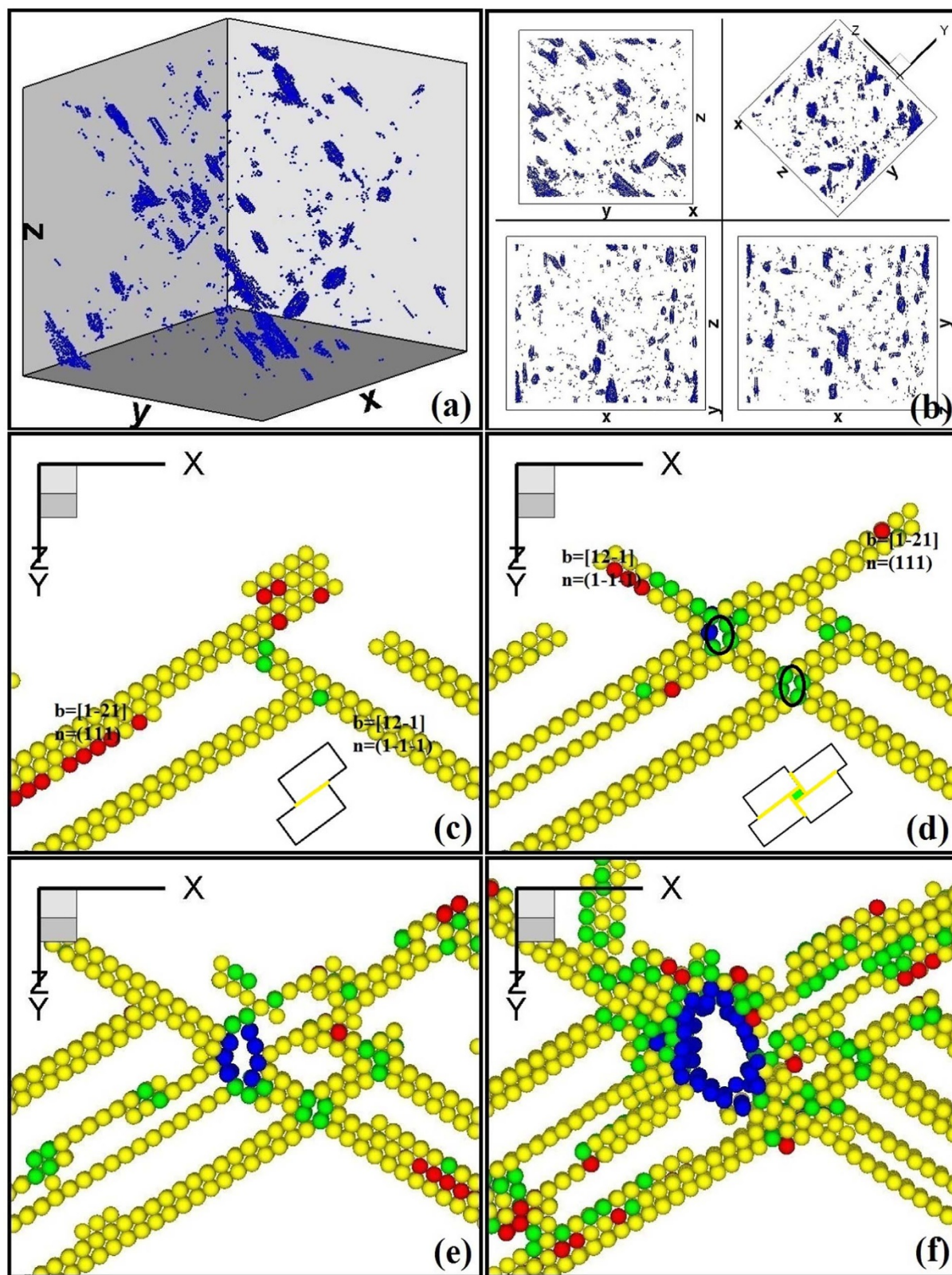


Figure 3 | Incipient void nucleation phenomenon and its two-stage mechanism. Panel (a) and (b) shows the void nucleation phenomenon. Panels (c)–(f) show the evolutionary process of these atoms in a picked slice, and therein the insets are the schematic diagrams of stacking faults creation and vacancy string formation. Panel (c) shows that four stacking faults appearing as lines nucleate from double-layer defect clusters. Panel (d) shows that two pillar-like vacancy strings are generated from the intersections of stacking faults, see the upper and lower black circles. Panel (e) shows that the upper vacancy string transforms into a void via emitting dislocations, while the lower one retains its size. Panel (f) shows that nucleated voids grow gradually and neighboring vacancy strings disappear.

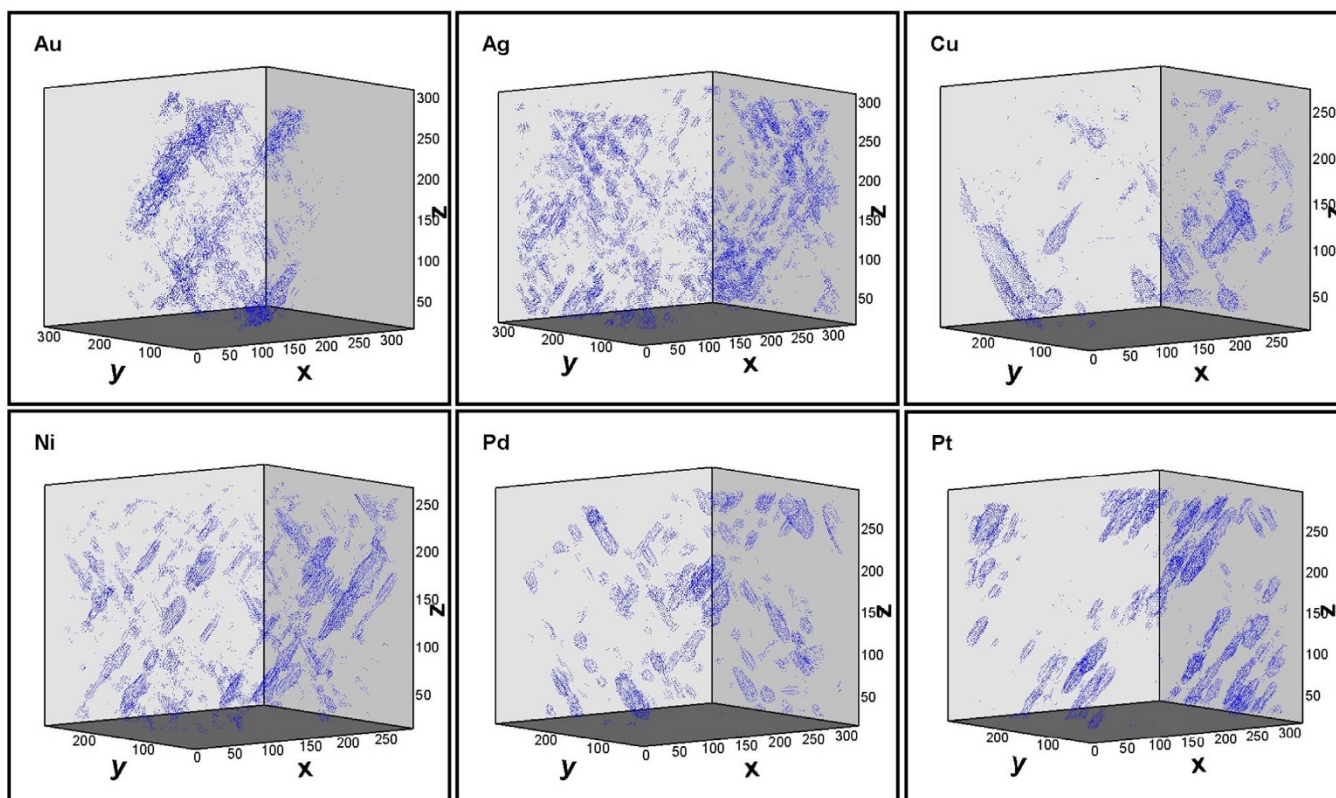


Figure 4 | Molecular-dynamics simulation results for shapes and distributions of nucleated voids in six different ductile metals.

during the plastic procedure. Whereas, for materials with high stacking fault energy, for example, the aluminum, initially created dislocations are almost perfect dislocations and nearly no stacking faults can be formed during the plastic procedure. In such materials, tensional loading with high strain rate generally leads to point defects or microcracks, instead of the voids. Therefore, the newly found mechanisms for dislocation creation and void nucleation in the present paper are valid for ductile metals with low stacking fault energies.

In conclusion, through systematic molecular dynamics simulations and a rationalized analysis on the evolution behavior of several typical FCC ductile metals under high-strain-rate uniaxial tension, we have provided a general physical picture for the dislocation creation and void nucleation. We have shown that the dislocation creation follows a three-stage procedure, in which random FOSs are at first activated by thermal fluctuations, then the FOSs form double-layer defect clusters via stacking on the close-packed planes, and finally these double-layer defect clusters evolve into Shockley partial dislocations due to relative slip of internal atoms. Whereas, the void nucleation follows a two-stage procedure, in which the first stage is characterized by the generation of pillar-like vacancy strings through intersections of different stacking faults, while the second stage is represented by transformation of vacancy strings perpendicular to the loading direction into voids via emitting dislocations. Our findings are expected to pave a way to build up a general microscopic understanding on the origin of dislocation creation and void nucleation in a variety of ductile metals, which we believe is fundamental for accurate dynamic damage fracture modeling.

Methods

Three methods have been employed in our numerical simulations and data analysis: (i) The numerical MD simulations are performed using the well-known LAMMPS software package. The interatomic interactions used in the simulations are described by embedded atom method potentials. The dilative strain is applied uniformly through re-scaling the coordinates as in the Parrinello-Rahman approach; (ii) The atoms are distinguished by the common neighbor analysis (CNA) method. In this

method the signature of the local crystal structure of an atom is identified by computing three characteristic numbers for each of the N neighbor bonds of the central atom; (iii) The Burgers vectors of the evolved dislocations in the MD simulations are calculated using our home-built code. In this code, dislocation lines and their directions are first identified. Then, surrounding the dislocation lines, appropriate Burgers circuits that cross stacking-fault planes or perfect crystal are selected, and the atom-to-atom sequences corresponding to the circuits are determined. Finally, after a summation over vectors of the Thompson's tetrahedron and its mirrors that are most closest to the atom-to-atom vectors, the Burgers vectors of the dislocations are obtained.

- Seaman, L., Curran, D. R. & Shockey, D. A. Computational models for ductile and brittle fracture. *J. Appl. Phys.* **47**, 4814–4826 (1976).
- Lubarda, V. A., Schneider, M. S., Kalantar, D. H., Remington, B. A. & Meyers, M. A. Void growth by dislocation emission. *Acta Mater.* **52**, 1397–1408 (2004).
- Seppala, E. T., Belak, J. & Rudd, R. E. Onset of Void Coalescence during Dynamic Fracture of Ductile Metals. *Phys. Rev. Lett.* **93**, 245503 (2004).
- Takahiro, H. Dislocation Nucleation in Shocked fcc Solids: Effects of Temperature and Preexisting Voids. *Phys. Rev. Lett.* **93**, 085501 (2004).
- Berk, H., Barend, J. T. & Erik, V. D. G. Molecular dynamics study of dislocation nucleation from a crack tip. *Phys. Rev. B* **71**, 054111 (2005).
- Zuo, L., Ngan, A. H. W. & Zheng, G. P. Size Dependence of Incipient Dislocation Plasticity in Ni_3Al . *Phys. Rev. Lett.* **94**, 095501 (2005).
- Douglas, E. S., Karl, I. J. & David, L. M. Nucleation of dislocations from $[0\ 0\ 1]$ bicrystal interfaces in aluminum. *Acta Mater.* **53**, 3579–3589 (2005).
- Swygenhoven, H. V., Derlet, P. M. & Fresset, A. G. Nucleation and propagation of dislocations in nanocrystalline fcc metals. *Acta Mater.* **54**, 1975–1983 (2006).
- Liu, Y. F., Erik, V. D. G. & Needleman, A. An analysis of dislocation nucleation near a free surface. *Int. J. Solids Struct.* **44**, 1719–1732 (2007).
- Zhu, T., Li, J., Samanta, A., Leach, A. & Gall, K. Temperature and Strain-Rate Dependence of Surface Dislocation Nucleation. *Phys. Rev. Lett.* **100**, 025502 (2008).
- Garrison, W. M. & Moody, N. R. Ductile fracture. *J. Phys. Chem. Solids.* **48**, 1035–1074 (1987).
- Srinivasan, S. G. & Baskes, M. I. Atomistic simulations of shock induced microstructural evolution and spallation in single crystal nickel. *J. Appl. Phys.* **101**, 043504 (2007).
- Dremov, V. *et al.* Molecular dynamics simulations of the initial stages of spall in nanocrystalline copper. *Phys. Rev. B* **74**, 144110 (2006).
- Dongare, A. M., Rajendran, A. M. & LaMattina, B. Atomic scale simulations of ductile failure micromechanisms in nanocrystalline Cu at high strain rates. *Phys. Rev. B* **80**, 104108 (2009).



15. Yuan, F. P. & Wu, X. L. Shock response of nanotwinned copper from large-scale molecular dynamics simulations. *Phys. Rev. B* **86**, 134108 (2012).
16. Belak, J. On the nucleation and growth of voids at high strain-rates. *J. Comput. Aided Mater. Design*. **5**, 193–206 (1998).
17. Plimpton, S. Fast Parallel Algorithms for Short-Range Molecular Dynamics. *J. Comp. Phys.* **117**, 1–19 (1995).
18. Daw, M. S. & Baskes, M. I. Embedded-atom method: Derivation and application to impurities, surfaces, and other defects in metals. *Phys. Rev. B* **29**, 6443 (1984).
19. Foiles, S. M., Baskes, M. I. & Daw, M. S. Embedded-atom-method functions for the fcc metals Cu, Ag, Au, Ni, Pd, Pt, and their alloys. *Phys. Rev. B* **33**, 7983 (1986).
20. Wang, S. C., Lu, G. & Zhang, G.-C. A Frank scheme of determining the Burgers vectors of dislocations in a FCC crystal. *Comp. Mater. Sci.* **68**, 396–401 (2013).

Acknowledgments

We acknowledge support of the National Magnetic Confinement Fusion Science Program in China (2012GB106001), the National Basic Security Research Program in China, and the National Natural Science Foundation in China under Grant No. 51071032.

Author contribution

W.W.P. did the calculations. P.Z., G.C.Z., A.G.X. and X.G.Z. analyzed the results. W.W.P., G.C.Z. and P.Z. wrote the paper. P.Z. and G.C.Z. were responsible for project planning and execution.

Additional information

Competing financial interests: The authors declare no competing financial interests.

How to cite this article: Pang, W.-W., Zhang, P., Zhang, G.-C., Xu, A.-G. & Zhao, X.-G. Dislocation creation and void nucleation in FCC ductile metals under tensile loading: A general microscopic picture. *Sci. Rep.* **4**, 6981; DOI:10.1038/srep06981 (2014).



This work is licensed under a Creative Commons Attribution-NonCommercial-ShareAlike 4.0 International License. The images or other third party material in this article are included in the article's Creative Commons license, unless indicated otherwise in the credit line; if the material is not included under the Creative Commons license, users will need to obtain permission from the license holder in order to reproduce the material. To view a copy of this license, visit <http://creativecommons.org/licenses/by-nc-sa/4.0/>